UNIVERSITY OF AMSTERDAM

UvA-DARE (Digital Academic Repository)

Heterogeneous distribution of prokaryotes and viruses at the microscale in a tidal sediment

Carreira, C.; Larsen, M.; Glud, R.N.; Brussaard, C.P.D.; Middelboe, M.

DOI
10.3354/ame01639

Publication date
2013

Document Version
Final published version

Published in
Aquatic Microbial Ecology

Link to publication

Citation for published version (APA):
Carreira, C., Larsen, M., Glud, R. N., Brussaard, C. P. D., & Middelboe, M. (2013). Heterogeneous distribution of prokaryotes and viruses at the microscale in a tidal sediment. *Aquatic Microbial Ecology*, *69*(3), 183-192. https://doi.org/10.3354/ame01639

General rights
It is not permitted to download or to forward/distribute the text or part of it without the consent of the author(s) and/or copyright holder(s), other than for strictly personal, individual use, unless the work is under an open content license (like Creative Commons).

Disclaimer/Complaints regulations
If you believe that digital publication of certain material infringes any of your rights or (privacy) interests, please let the Library know, stating your reasons. In case of a legitimate complaint, the Library will make the material inaccessible and/or remove it from the website. Please Ask the Library: https://uba.uva.nl/en/contact, or a letter to: Library of the University of Amsterdam, Secretariat, P.O. Box 19185, 1000 GD Amsterdam, The Netherlands. You will be contacted as soon as possible.

UvA-DARE is a service provided by the library of the University of Amsterdam (https://dare.uva.nl)

Download date:14 Nov 2026

Vol. 69: 183–192, 2013
doi: 10.3354/ame01639

AQUATIC MICROBIAL ECOLOGY
Aquat Microb Ecol

Published online June 14

FREE ACCESS

FEATURE ARTICLE

Heterogeneous distribution of prokaryotes and viruses at the microscale in a tidal sediment

Cátia Carreira[1,2], Morten Larsen[3,4,5], Ronnie N. Glud[3,4,5,6], Corina P. D. Brussaard[2], Mathias Middelboe[1,*]

[1]Section for Marine Biology, University of Copenhagen, Strandpromenaden 5, 3000 Helsingør, Denmark
[2]Department of Biological Oceanography, Royal Netherlands Institute for Sea Research (NIOZ), PO Box 50, NL 1790, AB Den Burg, The Netherlands
[3]Scottish Marine Institute, Scottish Association for Marine Science, Oban PA37 1QA, UK
[4]Institute of Biology and Nordic Center for Earth Evolution (NordCEE), University of Southern Denmark, 5320 Odense M, Denmark
[5]Greenland Climate Research Centre (CO Greenland Institute of National resources), Kivioq 2, Box 570, 3900 Nuuk, Greenland
[6]Arctic Research Center, University of Aarhus, 8000 Aarhus C, Denmark

ABSTRACT: In this study we show for the first time the microscale (mm) 2- and 3-dimensional spatial distribution and abundance of prokaryotes, viruses, and oxygen in a tidal sediment. Prokaryotes and viruses were highly heterogeneously distributed with patches of elevated abundances surrounded by areas of ca. 3-fold lower abundance within distances of <2 mm. Abundances of prokaryotes and viruses ranged from 1.3×10^9 to 4.2×10^9 cells cm^{-3} and 4.1×10^9 to 13.1×10^9 viruses cm^{-3}, respectively. The results showed oxygen concentration and uptake rates to be heterogeneously distributed at the same spatial scale, with the oxygen penetration depth varying from 1.5 to 5.8 mm and with an average (±SD) diffusive oxygen uptake of 18.9 ± 6.4 mmol m^{-2} d^{-1}. Locally, prokaryotes, viruses, and oxygen were found to be positively, negatively, or not correlated, but overall no significant relationship was detected. The lack of consistent spatial correlation between viruses and prokaryotes was explained by a temporal experiment using organic carbon-enriched homogenized sediment samples. Enhancement in metabolic activity and the proliferation of prokaryotes and viruses were not completely phased. These results suggest that local nourishment is likely to be an important driver of a high small-scale heterogeneity in abundance and dynamics of benthic viruses and prokaryotes. This is expected to influence the rates and regulation of benthic virus–host interactions and thus microbial biogeochemical cycling.

KEY WORDS: Spatial heterogeneity · Temporal dynamic · Hot spots · Virus–host interactions

Resale or republication not permitted without written consent of the publisher

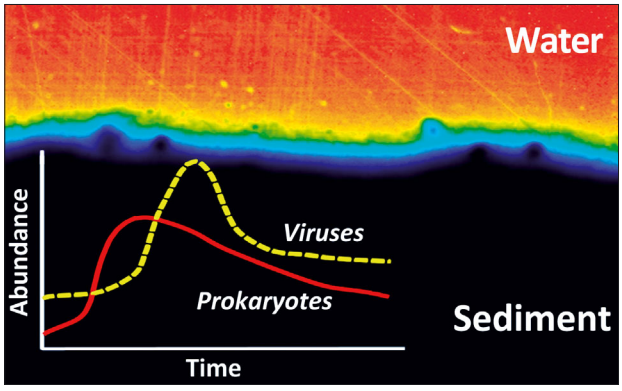

Oxygen distribution across the sediment–water interphase. Oxygen saturation varies from 0% (black) to 100% (red). Inset: temporal dynamics in prokaryote and viral abundance in response to organic carbon enrichment.

Image: Morten Larsen

INTRODUCTION

Virus abundance in marine sediments is generally 10 to 100 times higher than in the pelagic zone (Weinbauer 2004), yet still very little is known about their role in benthic environments. The conditions in sediments differ in many ways from those of free water masses, but 3 factors are of particular importance for prokaryote–virus interactions: sediments have an enormous surface area and low transport coefficients, and the volume-specific microbial activity of surface sediments is orders of magnitude higher than in water columns (Glud 2008).

*Corresponding author. Email: mmiddelboe@bio.ku.dk

© Inter-Research 2013 · www.int-res.com

Generally the abundance of viruses correlates positively with prokaryote abundance (e.g. Middelboe et al. 2006, Danovaro et al. 2008) and activity (Middelboe et al. 2003) in sediments, and viruses have been shown to be a dynamic component of microbial communities in marine sediments with potentially large impact on prokaryote mortality and biogeochemical cycling (Hewson et al. 2001, Fischer et al. 2003, Glud & Middelboe 2004).

Prokaryote and viral abundance normally decrease with sediment depth, as resolved by traditional vertical sediment slicing at cm to m resolution (e.g. Hewson et al. 2001, Glud & Middelboe 2004, Middelboe et al. 2011). Horizontally, viral distribution has been monitored along transects at spatial scales ranging from a few cm to km distance (e.g. Hewson et al. 2001, Middelboe & Glud 2006, Middelboe et al. 2006). These studies concluded that despite an overall positive relationship between trophic status and the abundance of prokaryotes and viruses, most of the variability is expressed on a much smaller spatial scale, with large differences in abundances of prokaryotes and viruses in sediment patches separated by a few cm (Hewson et al. 2001, Middelboe & Glud 2006, Middelboe et al. 2006). Since the microbial metabolic activity is driven by a highly patchy microscale distribution of both electron donors and acceptors (Fenchel & Glud 2000, Glud et al. 2009), none of these studies focused on the most relevant spatial scale for interactions between microbial communities and viruses.

Here we examined the small scale (mm) 2- and 3-dimensional spatial distribution and abundance of prokaryotes and viruses in combination with oxygen measurements in shallow coastal sediments to map small-scale distribution in microbial abundance and activity. Additionally, to resolve possible lack of correlation between virus and prokaryote abundance, we also examined successive changes in the abundance of prokaryotes and viruses in homogenized sediment samples as a function of the community metabolic activity.

MATERIALS AND METHODS

Study site and sediment characteristics

Sampling was conducted in November 2009 at low tide in Dunstaffnage Bay (West Coast of Scotland, 56° 27.0′ N, 5° 26.4′ W) at a water temperature of 9°C. The sediment was sampled using a custom made sampler, allowing the transfer of intact sediment cores into the flow chambers. Three cores were sampled and used for general characterization of sediment porosity and the content of organic matter. Briefly, 3 sediment cores were sampled and sliced every 0.5 cm to a maximum depth of 5 cm. Porosity (φ) was determined from the density and the weight loss after drying at 105°C for 24 h, and decreased from 0.6 v/v at the sediment surface to 0.40 v/v at 5 cm depth. The content of organic matter was measured from the weight loss of dried samples after combustion at 450°C for 24 h, and was highest in the top 0.5 cm (2.3% dry weight), gradually declining to ~1.7% at 5 cm depth. At the same time, undisturbed, intact sediment was sampled and immediately transferred into pre-constructed flow chambers (20 × 15 × 8 cm; H × L × W). Once in the laboratory, the sediment was kept submerged under re-circulating seawater at *in situ* temperature (9 ± 1°C) and O_2 concentration for 2 d before experiments were carried out.

Two experiments (2 dimensions, 2D; and 3 dimensions, 3D) were performed with the sediment. In each experiment, abundances of prokaryotes and viruses were measured in parallel to oxygen (O_2) concentrations and dynamics. The measurements of O_2 concentrations and dynamics were performed using planar optodes (2D) and microelectrodes (3D).

Planar optode imaging

The principles for planar optode imaging have been previously described in detail (Glud et al. 1996, Holst et al. 1998, Holst & Grunwald 2001) and are only briefly described below. The imaging system was based on a 1.3 megapixel fast gatable, 12-bit, Peltier cooled, charge-coupled device camera (SensiCam, www.PCO.de) equipped with a 25 mm/1.4 Nikon wide-angle lens equipped with 690 nm longpass dichroic color filter (UQG optics, www.UQGoptics.com) (Frederiksen & Glud 2006). Excitation light was delivered from 4 high power light-emitting diodes (LEDs, λ-peak = 445 nm, LXHL-LR3C, Luxeon, F = 340 mW at IF = 700 mA), equipped with a 475 nm short-pass dichroic color filter (UQG optics, www.UQGoptics.com). To allow measurements of the relatively short-lived phosphorescent lifetime, the camera and an LED power supply were synchronized with a custom made trigger box. The trigger box was connected to a PC and controlled by the software Look@Molli (Holst & Grunwald 2001). The phosphorescent lifetime was inferred from 2 well defined time frames configured by the Look@Molli software. Recorded images were calibrated using the

phosphorescent lifetime recorded in 2 areas where the foil was exposed to known O_2 concentrations (100% air saturation in the overlying water and 0% air saturation in deep anoxic sediment layers), and using a rearranged modified Stern-Volmer equation.

$$C = \frac{\tau_0 - \tau}{K_{SV} \cdot (\tau - \tau_0 \cdot \alpha)} \quad (1)$$

where τ_0 is the phosphorescent lifetime in the absence of O_2 and τ is the lifetime in the presence of any given oxygen concentration (C), K_{SV} is the bimolecular quenching constant, and α is the non-quenchable fraction of the phosphorescent signal, which was experimentally determined to be 0.14. All images were recorded in darkness to avoid potential interference from ambient light. Images were recorded using a 16 image average to increase the signal to noise ratio. The maximum theoretical spatial resolution that could be achieved with the given optical setup was ~100 × 100 µm.

Microelectrode profiling

O_2 profiles were measured by Clark-type microelectrodes equipped with an internal reference and a guard cathode (Revsbech 1989). The sensors had external tip diameters of 10 to 20 µm, a stirring sensitivity <2%, and a 90% response time of <1 s (Gundersen et al. 1998). The sensors were mounted on a motor-driven micromanipulator, and the sensor currents were measured using a picoammeter (PA 2000, Unisense) and transferred via an A/D-converter to a PC. The O_2 microprofiles were measured at a vertical resolution of 100 µm. The sensor values were calibrated against the known O_2 concentration of the overlying water and 0 values recorded in deep anoxic sediment layers. The diffusive oxygen uptake (DOU) was calculated using Fick's first law of diffusion, $J = D_0(dC/dz)$, where dC/dz is the O_2 concentration at a given depth within the diffusive boundary layer (DBL) and D_0 is the molecular diffusion coefficient corrected for salinity and temperature (Glud 2008). Two sensors were mounted on the micromanipulator, thus 2 independent profiles were acquired simultaneously. Profiling of the 30 samples took approximately 6 h. Contour plots were made in Surfer 9.0.

Small-scale spatial sampling of prokaryotes and viruses

Small-scale samples for prokaryote and viral abundance were taken using a purpose-designed minicore. The plastic minicore had an outer diameter of 3.6 mm and an inner diameter of 3.0 mm and a maximum length of 80 mm. As the objective of this study was to sample both in 2D and 3D, 2 different devices were used. For the 2D sampling, 9 minicores were fixed and aligned side by side separated by a center distance of 5.6 mm (Fig. 1A). The 9 cores penetrated the sediment to a maximum depth of 27 mm. A hand pump was used to maintain a vacuum and avoid displacement of sediment in the minicores, during recovery (each minicore was connected to the pump by a plastic tube). Each of the 9 minicores was sliced vertically at a depth resolution of 3 mm, with a total of 9 slices. Planar optode images were taken on the exact same location before sampling.

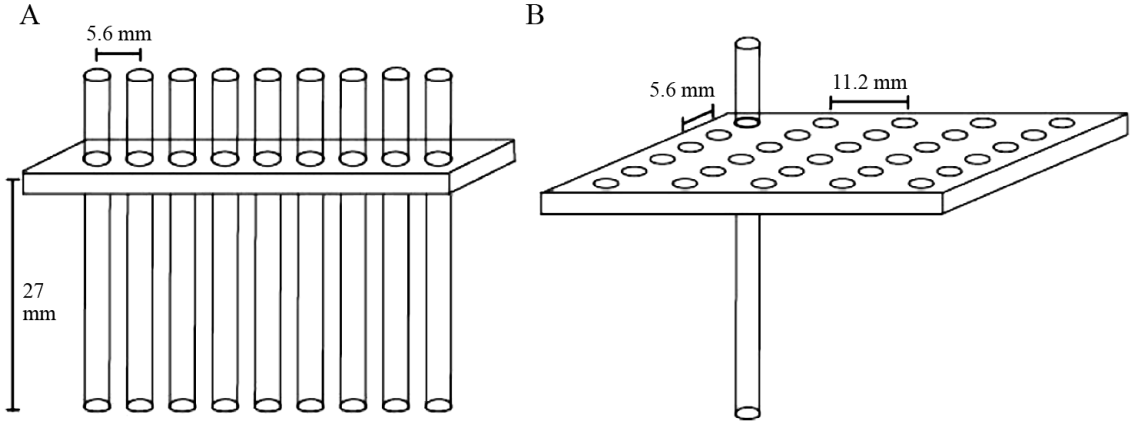

Fig. 1. Sampling devices. (A) Two-dimensional structure in which 9 minicores, separated by a center distance of 5.6 mm, were inserted down to 27 mm depth along a 47.8 mm transect. (B) Three-dimensional structure in which each minicore was inserted down to 6 mm depth, separated by an internal distance of 11.2 and 5.6 mm in length and width, respectively, in a total of 30 holes within 1481.8 mm^2

In the 3D experiment, the minicores were inserted one by one through a plexiglass plate with a grid of sampling holes (Fig. 1B). The plate was fixed to the wall of the flow channel, and a total of 30 minicores were recovered and separated from each other by an internal center distance of 11.2 and 5.6 mm in length and width, respectively. Each minicore was inserted to a depth of 6 mm and subsequently sliced in 2 depth intervals: 0–3 and 3–6 mm. Microelectrode profiling in the same grid holes was done prior to sampling.

Sample preparation and analysis of prokaryote and virus counts

Each sediment slice (~23 µl) was placed into a sterile 2 ml tube and fixed with 2% glutaraldehyde (final concentration) for 15 min at 4°C. The samples were then snap frozen in liquid nitrogen and kept at −80°C until further analysis. Prokaryotes and viruses were extracted from the sediment and treated according to Danovaro & Middelboe (2010) by the addition of tetrasodiumpyrophosphate (10 mM final concentration) in the dark for 15 min and sonicated using a probe sonicator (Sonicprep 150; 4 µm amplitude) in 3 cycles of 1 min sonication and 30 s of manual shaking in an ice bath. Then, 5 µl of the extract were diluted in 1 ml of 0.02 µm filtered seawater (virus free) and filtered onto a 0.02 µm Anodisc filter. Filters were stained in a drop of 10% SYBR Gold (Noble & Fuhrman 1998) for 15 min and subsequently rinsed 3 times in a series of MilliQ water drops. Finally, filters were mounted on a glass slide with an anti-fade solution (50% glycerol, 50% phosphate buffered saline pH = 7.5, 1% *p*-phenylendiamine) and preserved at −20°C. Prokaryotes and viruses were counted on an epifluorescence microscope (Olympus) at 600× to 750× magnification. Per sample, 400 prokaryotes and viruses or at least 10 fields were counted. Contour plots were made in Surfer 9.0.

Regression analyses were performed on prokaryote and virus abundance and O_2 concentration using the best fit between the 2 variables x and y obtained by regression model I as described by Sokal & Rohlf (1995). Normality was checked and the confidence level was set at 95% with all statistical analyses conducted in SigmaPlot 12.0.

Temporal dynamics in homogenized sediment

To understand the potential lack of correlation between prokaryotes and viruses, another experiment was established where prokaryote and viral abundance and production, and community respiration (dissolved inorganic carbon, DIC) were followed over time under enriched conditions at 2 different temperatures (8 and 13°C). The 2 temperatures were applied to determine whether the same temporal pattern in virus and prokaryote abundance developed at 2 different metabolic activity levels. Approximately 500 g of sediment from 3–6 cm depth was homogenized, enriched with yeast extract (~12.5 mmol C kg^{-1}), and transferred to duplicate gas-tight Würgler bags (Hansen et al. 2000) under a nitrogen atmosphere in a glove bag. Samples for prokaryote and viral abundance and DIC concentration were collected every 4 h for the first 24 h, after which the sampling frequency was reduced until the end of the experiment after 136 h. For practical purposes involving multiple sampling of the same homogenized sediment samples under anoxic conditions, and to overcome small-scale heterogeneity that may develop in the bags, a larger sediment volume was sampled (10 g) and processed according to Danovaro & Middelboe (2010). For DIC measurements, pore water from sediment was retrieved after centrifugation (2000 × *g*, 5 min), and preserved in 2 ml gas-tight vials containing 20 µl saturated $HgCl_2$ at 5°C until further analysis on an infrared gas analyzer (ADC-225-MK3; Glud & Middelboe 2004). Rates of respiration were calculated by linear regression of the increase in DIC concentration over time, whereas exponential rates of prokaryote and viral net production and decay were calculated by linear regression of changes in ln-transformed plots.

RESULTS

Microscale 2D spatial distribution

Oxygen images resolved an O_2 penetration depth (OPD) that varied from 1.5 to 2.3 mm along the primary interface (Fig. 2). As a result of irrigating fauna, a few patches of elevated O_2 concentration were observed in the deep otherwise anoxic sediment. The contour plots showed fine-scale variability in the distribution of prokaryotes and viruses (Fig. 3A,B) across distances as small as 2 mm over the 2D area sampled (1218 mm^2), i.e. 1.3×10^9 to 4.2×10^9 prokaryotes cm^{-3} and 4.1×10^9 to 11.3×10^9 viruses cm^{-3}, respectively. The spatial dispersal of both prokaryotes and viruses was characterized by patches with higher abundance surrounded by areas with 3-fold lower abundances. The distribution varied from

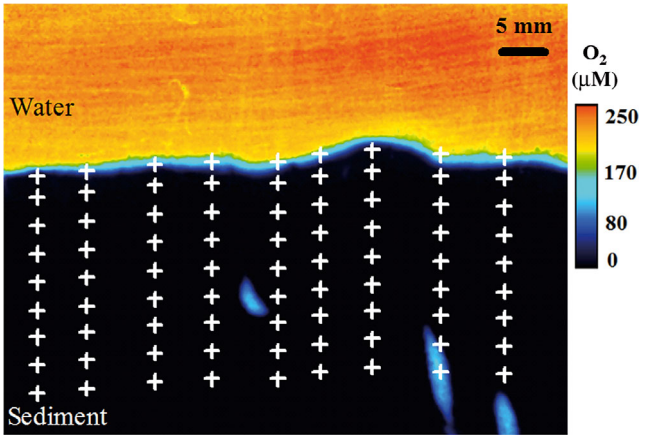

Fig. 2. Planar optode image representing the average 2-dimensional distribution of O_2 concentration in surface sediments as calculated from 166 optode images, recorded prior to the microscale sampling. Crosses represent the position of the microscale sampling for prokaryotes and viruses in the sediment with water above

similar patterns of prokaryotes and viruses (i.e. high prokaryote abundances associated with high viral abundances and vice versa) to opposite patterns (i.e. high prokaryotes–low viruses or low prokaryotes–high viruses; Fig. 3A,B).

The subsequent range in the virus to prokaryote ratio (VPR) was between 1.7 and 5.1, without a clear spatial pattern (Fig. 3C). Prokaryote abundance, viral abundance, and O_2 concentrations did not exhibit statistically significant correlations ($p > 0.05$, $n = 83$).

Microscale 3D spatial distribution

The small-scale variability in O_2 distributions (Fig. 2) was also reflected in the O_2 microprofiles (Fig. 4) measured across a horizontal grid in the 3D study. OPD varied between 2.3 and 5.8 mm, with O_2 concentrations ranging from 40 to 139 µM in the top layer (0–3 mm; Fig. 5A). O_2 concentration in the bottom layer (3–6 mm; Fig. 5B) was mostly <1 µM, although areas with elevated O_2 concentration were observed in a few profiles. The mean diffusive O_2 uptake derived from the O_2 concentration gradient of the DBL was 18.9 ± 6.4 mmol m^{-2} d^{-1}, which is a typical value for coastal marine sediments (Glud 2008).

Prokaryote and viral abundances in the top layer (0–3 mm) varied from 1.4 × 10^9 to 2.8 × 10^9 cells cm^{-3} and 4.4 × 10^9 to 13.1 × 10^9 viruses cm^{-3}, respectively (Figs. 6A & 7A). In the bottom layer (3–6 mm), they ranged from 1.5 × 10^9 to 3.3 × 10^9 prokaryotes cm^{-3} and 4.4 × 10^9 to 12.8 × 10^9 viruses cm^{-3} (Figs. 6B & 7B). The spatial distribution was characterized by areas of elevated prokaryote or viral abundance occurring next to low-density areas within a few mm distance.

Comparing the spatial distribution of prokaryotes and viruses in the top layer (0–3 mm, Figs. 6A & 7A) showed a few locations with similar patterns (high prokaryotes–high viruses or low prokaryotes–low viruses), but mostly there was a spatial uncoupling of prokaryote and viral

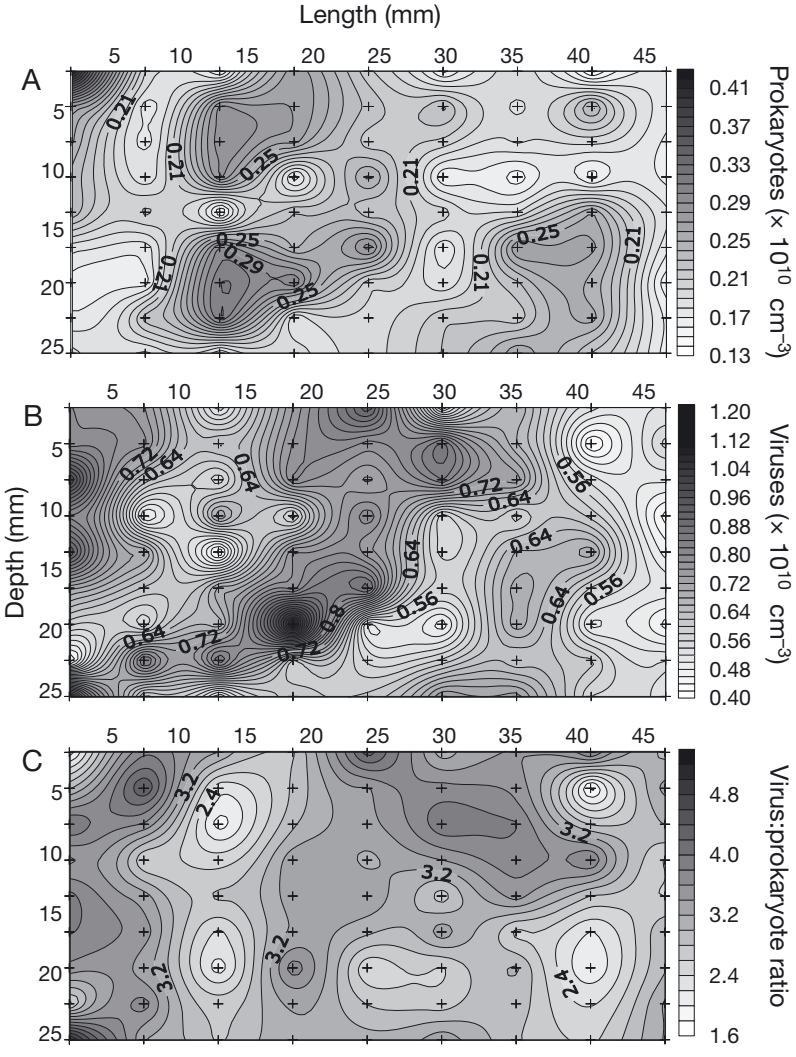

Fig. 3. Two-dimensional (47.8 × 25.5 mm) distribution and concentration of (A) prokaryote abundance, (B) viral abundance, and (C) virus: prokaryote ratio in tidal sediment. Crosses represent the position of the microscale sampling

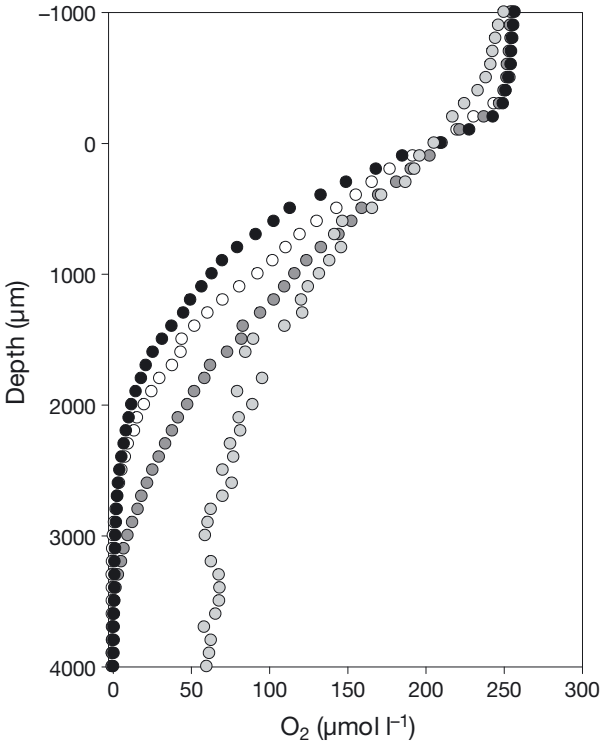

Fig. 4. Representative O_2 profiles recorded with the microelectrode from the 3-dimensional experiment. Symbols represent individual O_2 profiles. Profiles were recorded in all sampling spots prior to sampling. The position $y = 0$ represents the sediment surface

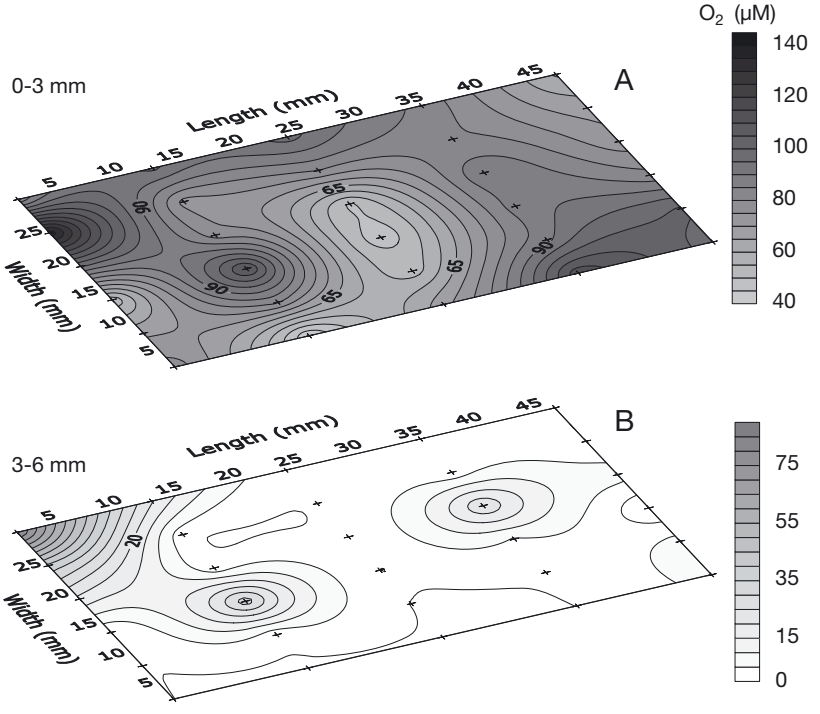

Fig. 5. Three-dimensional (47.8 × 31.6 × 6 mm) average O_2 concentration in the (A) 0–3 mm and (B) 3–6 mm sediment layer, composed of 30 individual microelectrode profiles. Crosses represent positions of the individual O_2 profiles

abundance (high prokaryotes–low viruses; low prokaryotes–high viruses), and overall, no significant correlation between prokaryotes and viruses or oxygen was observed ($p > 0.05$, $n = 26$). In the bottom layer (3–6 mm), viral abundances tended to follow the prokaryote distribution (Figs. 6B & 7B), although the relationship between prokaryotes and viruses in this anoxic layer overall was not significant ($p > 0.05$, $n = 27$).

The VPR was rather similar in the oxic and the anoxic layer, varying from 2.7 to 5.8 in the surface layer (Fig. 8A) and from 2.6 to 5.2 in the bottom layer (Fig. 8B). The experiment was repeated using a parallel sediment sample, which showed a similar spatial heterogeneity in viral and prokaryote abundances (data not shown).

Temporal dynamics in homogenized sediment

Changes in prokaryote and viral abundances in response to community respiration were examined in enriched, homogenized sediment to explore possible mechanisms for the observed spatial uncoupling between their abundances in natural sediments. The rates of change in prokaryote and viral abundance and community respiration varied considerably and systematically over the 4 main time periods in both experiments, exhibiting the same temporal pattern at both temperatures (Fig. 9A,B). In the initial period (0–8 h), prokaryotes, viruses, and DIC increased, followed by a decrease in prokaryote net production, whereas viral abundance continued to increase (8–20 h). Thereafter (20–38 h), prokaryote net production ceased concomitant with net decay in viral abundance despite relatively high community respiration. By the end of the experiment (38–135 h), the incubations reached stationary phase without significant rates of changes in abundances or activities.

As a consequence of these differences in the successions of prokaryotes and viruses, the VPR increased from ~4 to 5.5 during the first 20 h of the incubation and then rapidly declined to around 3 (Fig. 9C), thus covering the range of VBR obtained in the spatial study (Figs. 3C & 8).

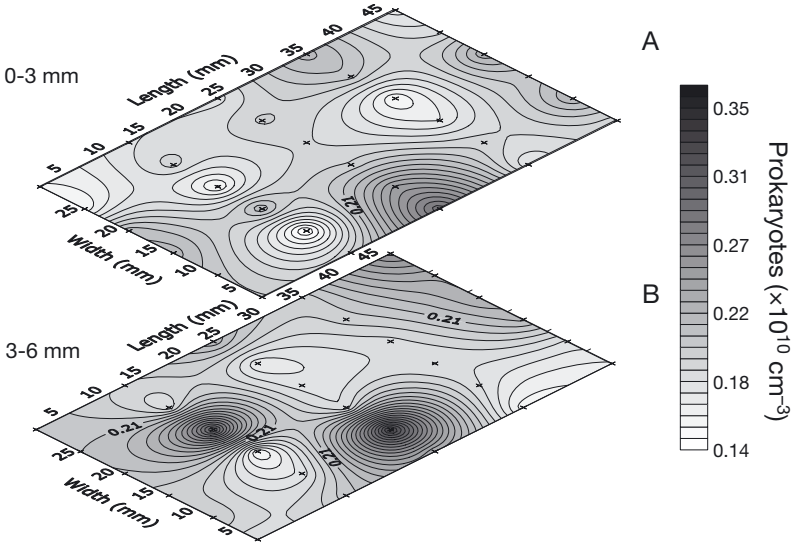

Fig. 6. Three-dimensional (47.8 × 31.6 × 6 mm) distribution of prokaryote abundance in the (A) 0–3 mm and (B) 3–6 mm sediment layer. Crosses represent the position of the microscale sampling

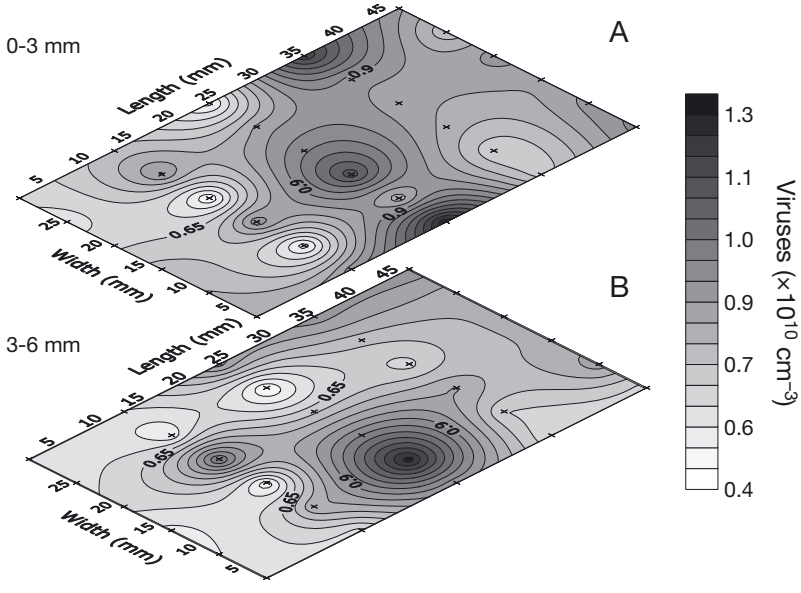

Fig. 7. Three-dimensional (47.8 × 31.6 × 6 mm) distribution of viral abundance in the (A) 0–3 mm and (B) 3–6 mm sediment layer. Crosses represent the position of the microscale sampling

DISCUSSION

Here we showed that prokaryotes and viruses in tidal sediments are highly heterogeneously distributed even at the mm scale. Until now, spatial variations in prokaryote and viral abundances have always been monitored in homogenized sediment samples at cm to m scale resolution, and reported values have typically represented average abundances in 30–100 cm^3 sediment slices (Hewson et al. 2001, Glud & Middelboe 2004). On these spatial scales, significant decreases in viral abundance and production have been observed with sediment depth or along trophic gradients (e.g. Hewson et al. 2001, Middelboe & Glud 2006, Middelboe et al. 2011), reflecting reduced microbial activity as availability of organic matter declines, and suggesting prokaryote abundance and metabolic activity as predictors of viral dynamics.

However, benthic microbial and viral dynamics occur on a much smaller scale and are considered to be related to microniches induced by e.g. sedimentation of aggregates and faunal activity (Fenchel & Glud 2000, Glud et al. 2009). At this spatial scale, our data revealed a highly heterogeneous distribution of microbial abundances and oxygen concentration in the upper 27 mm of a temperate, coastal tidal sediment with areas of elevated abundances (hotspots) extending a few mm in vertical and horizontal directions. Prokaryote and viral abundance did not correlate across the vertical and horizontal gradients analyzed, and no clear vertical or horizontal patterns in their distribution were observed at this spatial resolution within the investigated sampling grids. Consequently, small-scale viral distribution and the relation to the activity and abundance of their prokaryote hosts followed a highly different pattern than the distribution patterns obtained from homogenized sediment samples on large spatial scales. The small-scale spatial variation found in this study thus supports the accumulating evidence of highly heterogeneous microscale distribution of organic matter (Fenchel 2008) and microbial diagenetic activity in surface sediments as resolved by O_2 and DIC measurements obtained using microsensors and targeted incubation approaches (Fenchel & Glud 2000).

Our observations are in line with the 2D distribution of prokaryotes and viruses obtained at a similar spatial scale in pelagic environments (Seymour et al. 2006, 2008), demonstrating an equally heterogeneous and non-correlated distribution of prokaryotes and viruses, which is consistent with observations of organic matter heterogeneously distributed in aggregates providing microzones of elevated prokaryote activity (Blackburn et al. 1998). A similar heterogeneous horizontal distribution of bacterial abundance was observed at the cm scale in a coastal surface sediment without any correlation to the distribution of their potential food sources, suggesting a time lag between organic matter input and the microbial response (Danovaro et al. 2001). The present study thus emphasizes that microscale microbial dynamics and local diagenetic hotspots are an inherent feature of marine ecosystems, which should be better recognized when evaluating dynamics in diagenetic processing and microbial community distribution.

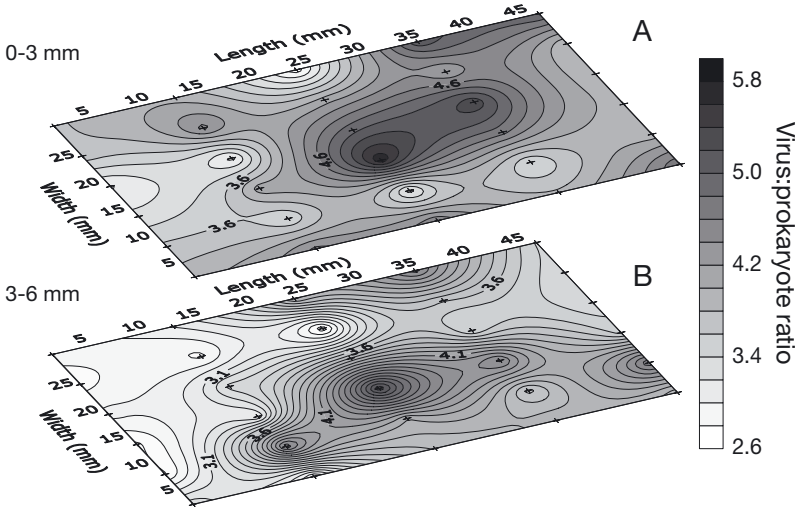

Fig. 8. Three-dimensional (47.8 × 31.6 × 6 mm) distribution of virus:prokaryote ratio (VPR) in the (A) 0–3 mm and (B) 3–6 mm sediment layer. Crosses represent the position of the microscale sampling

Viral replication may depend strongly on its host metabolic activity, and thus elevated viral abundances are theoretically expected in association with observed niches of intensified prokaryote activity (Glud et al. 2005). However,

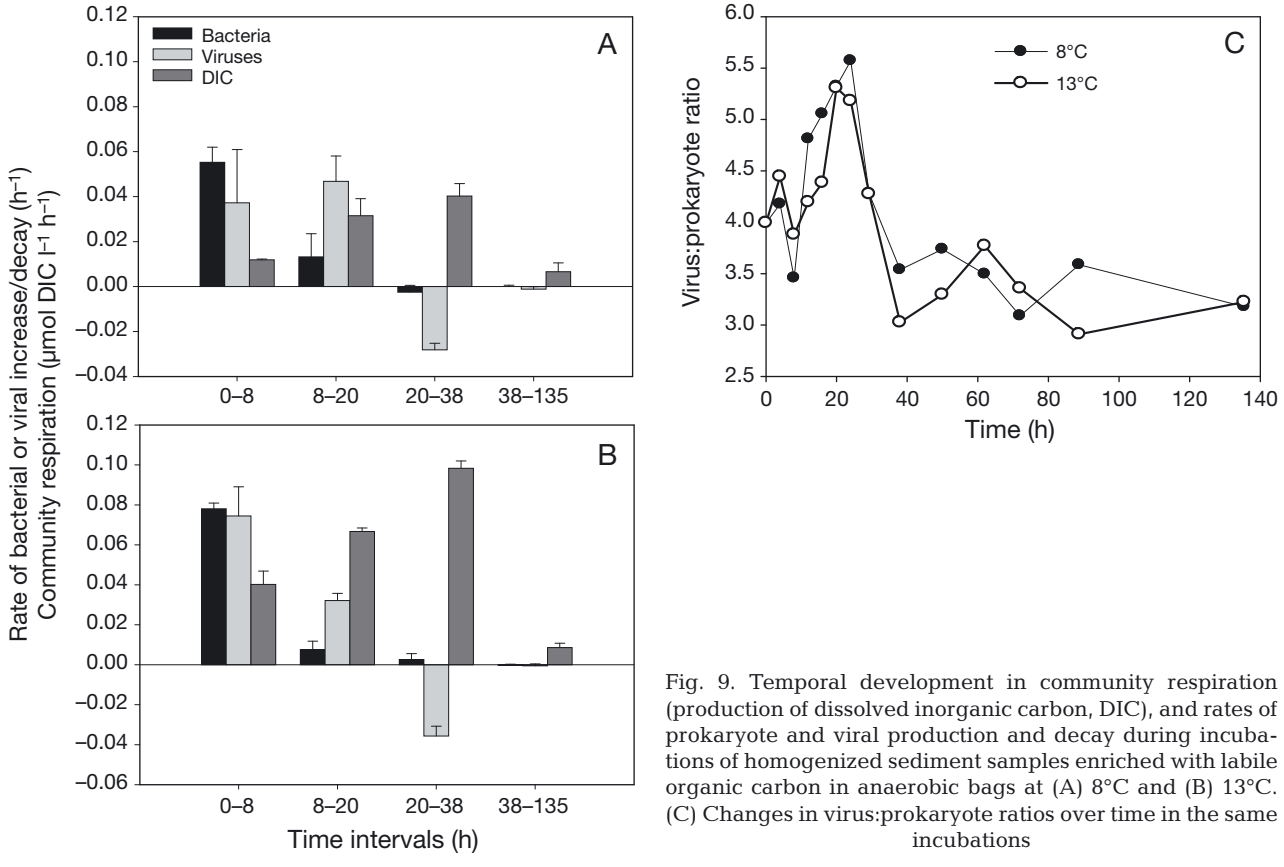

Fig. 9. Temporal development in community respiration (production of dissolved inorganic carbon, DIC), and rates of prokaryote and viral production and decay during incubations of homogenized sediment samples enriched with labile organic carbon in anaerobic bags at (A) 8°C and (B) 13°C. (C) Changes in virus:prokaryote ratios over time in the same incubations

due to the time lag from infection to viral proliferation, and to a variable life time of prokaryote and viral particles in the environment, abundances of prokaryotes and viruses may be uncoupled in time and space. Their distribution thus reflects the recent history of the specific environment rather than the actual activity of the microhabitat. The examination of temporal dynamics in net prokaryote and viral production and community respiration in homogenized sediment indeed showed an uncoupling over time in microbial abundances related to prokaryote activity in response to organic carbon enrichment. A sequence of events in response to local sediment enrichment resulted in a temporal uncoupling between viral and prokaryote abundances in the homogenized sediment, leading to 4 distinct scenarios of virus–prokaryote interactions within 48 h: (1) high prokaryote abundance and low viral abundance (0–8 h) as a result of the initial stimulation of prokaryote activity and a delay in the subsequent viral production, (2) high virus:prokaryote ratio due to a bloom of viruses in response to the elevated prokaryote activity (8–20 h), (3) high prokaryote abundance but low viral abundance reflecting a fast decay or irreversible particle-attachment of viruses following the bloom conditions (20–38 h), and (4) low prokaryote and viral abundance during the period of low microbial activity and reduced contact rates (>38 h).

The study validated that pulses of viral production and decay may indeed occur in response to local organic enrichment in marine sediments creating transient hotspots of elevated viral abundances associated with stimulation of prokaryote activity (Glud & Middelboe 2004, Siem-Jørgensen et al. 2008). We therefore suggest that the uncoupled microbial abundances and heterogeneous distribution of prokaryotes and viruses at the mm scale in surface sediments are driven by the dynamics of formation and degradation of patches of labile organic matter in the sediment, which stimulates prokaryote respiration and abundance and subsequently viral abundance. The traditional use of larger-scale samples averages out this microscale variability, which may have important implications for ecology at the fine scale relevant for the microbial communities in the sediment.

On a large spatial scale, the positive correlation between viral and prokaryote abundance and activity suggests that the general level of viral abundance in a given benthic environment is constrained by the levels of average microbial activity in that same environment. On a microscale, on the other hand, the lack of correlation suggests that virus–prokaryote interactions occur as periodic elevations and declines of viral and prokaryote densities associated with a continuous redistribution of microscale resource patches. Microscale variability in microbial distribution and dynamics has implications for microbial biogeochemical cycling that extends beyond the specific microhabitat, ultimately determining benthic carbon cycling on a global scale. Caution is therefore required when assessing the role of viruses from studies of viral and prokaryote activity based on homogenized samples, and there is a need for development of methods to measure *in situ* viral production at the scale and conditions at which they occur.

Acknowledgements. The study received financial support from the National Environmental Research Council (NERC: NE/F018614/1 and NE/F0122991/1), the Commission for Scientific Research in Greenland (KVUG: GCRC6507), the Danish National Research Foundation (DNRF53), the Danish Council for Independent Research (FNU-09-072829), The Carlsberg Foundation, ERC Advanced Grant (ERC-2010-AdG_20100224), and the Fundação para a Ciência e a Tecnologia (FCT: SFRH/BD/43308/2008).

LITERATURE CITED

Blackburn N, Fenchel T, Mitchell J (1998) Microscale nutrient patches in planktonic habitats shown by chemotactic bacteria. Science 282:2254–2256

Danovaro R, Middelboe M (2010) Separation of free virus particles from sediments in aquatic systems. Man Aquat Vir Ecol Chapt 8:72–79

Danovaro R, Armeni M, Dell'Anno A, Fabiano M and others (2001) Small-scale distribution of bacteria, enzymatic activities, and organic matter in coastal sediments. Microb Ecol 42:177–185

Danovaro R, Dell'Anno A, Corinaldesi C, Magagnini M, Noble R, Tamburini C, Weinbauer M (2008) Major viral impact on the functioning of benthic deep-sea ecosystems. Nature 454:1084–1087

Fenchel T (2008) Motility of bacteria in sediments. Aquat Microb Ecol 51:23–30

Fenchel T, Glud RN (2000) Benthic primary production and O_2-CO_2 dynamics in a shallow-water sediment: spatial and temporal heterogeneity. Ophelia 53:159–171

Fischer UR, Wieltschnig C, Kirschner AKT, Velimirov B (2003) Does virus-induced lysis contribute significantly to bacterial mortality in the oxygenated sediment layer of shallow oxbow lakes? Appl Environ Microbiol 69: 5281–5289

Frederiksen MS, Glud RN (2006) Oxygen dynamics in the rhizosphere of *Zostera marina*: a two-dimensional planar optode study. Limnol Oceanogr 51:1072–1083

Glud RN (2008) Oxygen dynamics of marine sediments. Mar Biol Res 4:243–289

Glud RN, Middelboe M (2004) Virus and bacteria dynamics of a coastal sediment: implication for benthic carbon cycling. Limnol Oceanogr 49:2073–2081

Glud RN, Ramsing NB, Gundersen JK, Klimant I (1996) Planar optodes: a new tool for fine scale measurements of

two-dimensional O_2 distribution in benthic communities. Mar Ecol Prog Ser 140:217–226

Glud RN, Wenzhöfer F, Tengberg A, Middelboe M, Oguri K, Kitazato H (2005) Distribution of oxygen in surface sediments from central Sagami Bay, Japan: in situ measurements by microelectrodes and planar optodes. Deep-Sea Res I 52:1974–1987

Glud RN, Stahl H, Berg P, Wenzhöfer F, Oguri K, Kitazato H (2009) In situ microscale variation in distribution and consumption of O_2: a study from a deep ocean margin sediment (Sagami Bay, Japan). Limnol Oceanogr 54:1–12

Gundersen JK, Ramsing NB, Glud RN (1998) Predicting the signal of oxygen microsensors from physical dimensions, temperature, salinity, and oxygen concentrations. Limnol Oceanogr 43:1932–1937

Hansen JW, Thamdrup B, Jørgensen BB (2000) Anoxic incubation of sediment in gas-tight plastic bags: a method for biogeochemical process studies. Mar Ecol Prog Ser 208:273–282

Hewson I, O'Neil JM, Fuhrman JA, Dennison WC (2001) Virus-like particle distribution and abundance in sediments and overlying waters along eutrophication gradients in two subtropical estuaries. Limnol Oceanogr 46: 1734–1746

Holst G, Grunwald B (2001) Luminescence lifetime imaging with transparent oxygen optodes. Sens Actuators B Chem 74:78–90

Holst G, Kohls O, Klimant I, König B, Kühl M, Richter T (1998) A modular luminescence lifetime imaging system for mapping oxygen distribution in biological samples. Sens Actuators B Chem 51:163–170

Middelboe M, Glud RN (2006) Viral activity along a trophic gradient in continental margin sediments off central Chile. Mar Biol Res 2:41–51

Middelboe M, Glud RN, Finster K (2003) Distribution of viruses and bacteria in relation to diagenetic activity in an estuarine sediment. Limnol Oceanogr 48: 1447–1456

Middelboe M, Glud RN, Wenzhöfer F, Oguri K, Kitazato H (2006) Spatial distribution and activity of viruses in the deep-sea sediments of Sagami Bay, Japan. Deep-Sea Res I 53:1–13

Middelboe M, Glud RN, Filippini M (2011) Viral abundance and activity in the deep sub-seafloor biosphere. Aquat Microb Ecol 63:1–8

Noble RT, Fuhrman JA (1998) Use of SYBR Green I for rapid epifluorescence counts of marine viruses and bacteria. Aquat Microb Ecol 14:113–118

Revsbech NP (1989) Diffusion characteristics of microbial communities determined by use of oxygen microsensors. J Microbiol Methods 9:111–122

Seymour JR, Seuront L, Doubell M, Waters RL, Mitchell JG (2006) Microscale patchiness of virioplankton. J Mar Biol Assoc UK 86:551–561

Seymour JR, Seuront L, Doubell MJ, Mitchell JG (2008) Mesoscale and microscale spatial variability of bacteria and viruses during a *Phaeocystis globosa* bloom in the eastern English Channel. Estuar Coast Shelf Sci 80: 589–597

Siem-Jørgensen M, Glud RN, Middelboe M (2008) Viral dynamics in a coastal sediment: seasonal pattern, controlling factors and relations to the pelagic-benthic coupling. Mar Biol Res 4:165–179

Sokal RR, Rohlf FJ (eds) (1995) Biometry the principles and practice of statistics in biological research. WH Freeman, New York, NY

Weinbauer MG (2004) Ecology of prokaryotic viruses. FEMS Microbiol Rev 28:127–181

Editorial responsibility: Gunnar Bratbak, Bergen, Norway

Submitted: February 6, 2013; Accepted: May 8, 2013
Proofs received from author(s): May 29, 2013